Effect of dolomite decomposition under CO_2 on its multicycle CO_2 capture behaviour under Calcium Looping conditions

Antonio de la Calle Martos[1, 2], *Jose Manuel Valverde*[2*], *Pedro E. Sanchez-Jimenez*[1], *Antonio Perejón*[1, 3], *Cristina García-Garrido, Luis A. Perez-Maqueda*[1].

[1] Instituto de Ciencia de Materiales de Sevilla, C.S.I.C.-Universidad de Sevilla, C. Américo Vespucio nº49, 41092 Sevilla, Spain.

[2] Faculty of Physics, University of Seville, Avenida Reina Mercedes s/n, Sevilla, Spain.

[3] Departamento de Química Inorgánica, Facultad de Química, Universidad de Sevilla, Sevilla, Spain.

Abstract

One of the main drawbacks that hinder the industrial competitiveness of the Calcium Looping (CaL) process for CO_2 capture is the high temperatures (~930-950ºC) needed in practice to attain full calcination of limestone under a high CO_2 partial pressure environment for short residence times as required in practice. In this work, the multicycle CO_2 capture performance of dolomite and limestone is analysed under realistic CaL conditions and using a reduced calcination temperature of 900ºC, which would serve to mitigate the energy penalty caused by integrating the CaL process into fossil fuel fired power plants. The results show that the fundamental mechanism of dolomite decomposition under CO_2 has a main influence on its superior performance compared to limestone. The inert MgO grains resulting from dolomite decomposition help preserving a nanocrystalline CaO structure wherein carbonation in the solid-state diffusion controlled phase is promoted. The major role played by dolomite decomposition mechanism under CO_2 is clearly demonstrated by the multicycle CaO conversion behaviour observed for samples decomposed at different preheating rates. Limestone decomposition at slow heating rates yields a highly crystalline and poorly reactive $CaCO_3$ structure that requires long periods to fully decarbonate and shows a severely reduced capture capacity in subsequent cycles. On the other hand, the nascent $CaCO_3$ produced after dolomite half-decomposition consists of nanosized crystals with a fast decarbonation kinetics regardless of the preheating rate, thus fully decomposing from the very first cycle at a reduced calcination temperature into a CaO skeleton with enhanced reactivity as compared to limestone derived CaO.

[*]Corresponding author. Tel +34 954550960
e-mail address: jmillan@us.es

1. Introduction

The interest in the Calcium looping (CaL) process as a cost-effective technology to mitigate post-combustion CO_2 emissions has generated a huge body of research oriented towards gaining a fundamental understanding on the calcination/carbonation reaction mechanism as well as to find the optimum operation conditions within the process constraints that serve to enhance CO_2 capture [1-6]. Despite the constant search for alternative Ca-based synthetic sorbents with enhanced thermal stability, natural limestone ($CaCO_3$) and dolomite ($CaMg(CO_3)_2$) still stand as the only practical CaO precursor due to their low cost (~10$/ton) and geographically spread wide availability [7]. In the typical CaL process, limestone is precalcined to produce CaO particles that will be subsequently used to capture CO_2 from the post-combustion gas stream by gas-solid reaction in a fluidised gas-solid reactor (carbonator) at temperatures of about 650 ºC. The partially carbonated particles are then transported into a second reactor (calciner) where CaO is regenerated by calcination at high temperatures (~930-950ºC) under high CO_2 partial pressure. In this way, a high CO_2 concentration stream can be retrieved from the calciner for compression and storage or other uses. Thus, the sorbent undergoes repeated carbonation/calcinations (carb/calc) cycles while it is circulated between the calciner and the carbonator [1, 7-10].

The CaL process presents two important drawbacks that challenge its technological development. Firstly, the high temperature required to achieve a complete regeneration of the sorbent in short residence times since calcination has to be carried out under the high CO_2 partial pressure calciner environment [11-14]. Such high temperatures would be attained by oxy-combustion in order to avoid CO_2 dilution, which entails a marked energy penalty to the process due to fuel consumption and additional CO_2 production [9, 10, 14-18]. The second inconvenient is the progressive deactivation of the sorbent along the successive carb/calc cycles that makes necessary to periodically introduce a fresh limestone makeup into the calciner. CaO deactivation may occur due to the screening effect of external agents such as ash or SO_2 produced during oxycombustion, which leads to the irreversible sulphation of the CaO particles [9, 13, 19, 20]. Yet, deactivation is mostly caused by the drastic loss of surface area of the CaO grains when calcination takes place under high CO_2 partial pressure and high temperatures, which enhances aggregation and subsequent sintering of the nascent CaO nanocrystals during the $CaCO_3$/CaO transformation [21].

Several methods have been proposed to mitigate deactivation of limestone derived CaO such as thermal pretreatment for prolonged periods [22-27]. However, thermal pretreatment does not yield CaO reactivation when the CaL cycles are carried out at realistic conditions for CO_2 capture, which necessarily involve calcination under high CO_2 partial pressure at high

temperatures and quick transitions between the carbonation and calcination stages. Only if a short recarbonation stage is introduced between carbonation and calcination, prolonged thermal pretreatment would lead to a substantial reactivation of the sorbent although it would require the use of an additional reactor [26]. On the other hand, it has been observed that the type of atmosphere under which limestone is first calcined plays a relevant role on the subsequent multicycle CaO behaviour. Thus, a quick precalcination in air produces a very porous CaO skeleton with high initial carbonation activity but also very prone to intense sintering when regenerated under a CO_2 rich atmosphere, thus exhibiting a severe drop of the CO_2 capture capacity after the very first cycles. Alternatively, a short precalcination of limestone under high CO_2 partial pressure, as would be the case if the solids makeup are directly fed into the calciner, yields a sorbent with a lower initial reactivity but also with a lower deactivation rate [28].

In recent publications, it has been shown that dolomite, ($CaMg(CO_3)_2$), also a widely available and cheap CaO precursor, exhibits higher CO_2 capture capacity and reduced deactivation as compared to limestone at realistic CaL conditions. This enhanced performance has been attributed to the superior resistance of CaO to sinter due to the inert skeleton of MgO grains that forms during first calcination of dolomite and over which the $CaO/CaCO_3$ layer builds up and decomposes during the subsequent carb/calc cycles [29-31]. Moreover, dolomite displays faster decarbonation kinetics thus allowing for a reduction of the temperature required for a complete CaO regeneration in the calciner in short residence times. This outstanding behaviour would serve to mitigate the energy penalty of the CaL process thus helping its industrial competitiveness. On the other hand, dolomite shows less resistance to attrition as compared to limestone although most of the attrition takes place during the first calcination [29].

In situ X-ray diffraction (XRD) coupled to thermogravimetric (TG) analysis has revealed that the mechanism of dolomite decomposition under CO_2 is responsible for enhancing the kinetics of calcination and reactivity of dolomitic CaO [21, 32]. Thus, dolomite decomposes directly into MgO and CaO at a temperature about 700ºC regardless of the CO_2 partial pressure in the calcination environment. If calcination is carried out under high CO_2 partial pressure (as is the case of the CaL process), the nascent CaO nanocrystals become immediately recarbonated, which leads to the formation of nanocrystalline calcite ($CaCO_3$) as intermediate product of decomposition. Because it consists of nanometer sized crystals, this nascent calcite rapidly decomposes when the reaction is thermodynamically favourable near 900ºC under high CO_2 partial pressure, yielding a nanocrystalline and therefore highly reactive CaO [21].

In this work, we explore the effect of different thermal pretreatments on the multicycle CO_2 capture performance of both limestone and dolomite at CaL conditions for CO_2 capture and using a calcination temperature of just 900ºC, which is about 30-50ºC below the typical calciner temperature employed for limestone in pilot-scale plants [33]. The results of our study will

serve to highlight the main role played by the fundamental mechanism of dolomite decomposition on its superior multicycle capture performance as compared to limestone.

2. Experimental

The experiments in this work have been carried out using a high purity natural limestone (99.6% $CaCO_3$) from Matagallar quarry (Pedrera, Spain) with an average particle size of 9.5 μm (volume-weighted mean particle size) and natural dolomite from Bueres (Spain). Raw dolomite was sieved to remove particles over 45 μm in order to avoid decrepitation phenomena during thermal decomposition, which may be significant for larger particles [34]. Phase quantification by Rietveld analysis showed the dolomite to have a purity of 94.4%, the rest being mostly calcite.

The multicycle CO_2 capture behaviour of the different sorbents was studied using a Q5000IR TG analyser (TA instruments) with high sensitivity ($< 0.1\mu g$). This instrument is equipped with a furnace heated by halogen lamps that allows for high heating/cooling rates up to 300ºC/min without significant fluctuations. This way, several consecutive carbonation/calcinations (carb/calc) cycles at different temperatures can be programmed with very quick transitions between stages thereby minimizing non-realistic reactions during the ramps as would happen in conventional furnaces, which are typically limited to heating rates below 25ºC/min. Achieving fast transitions between the carbonation and calcination stages is especially important when the sorbent is regenerated under high CO_2 partial pressure, as is the case of the CaL process for CO_2 capture. Otherwise, appreciable recarbonation occurs if the partially carbonated sorbent is slowly heated up to the high T isothermal plateau, which has a relevant influence on the sorbent behaviour in subsequent cycles. In order to avoid undesired effects due to CO_2 diffusion resistance through the bulk of the powder, samples of small mass (10 mg) were used. In this way, a high gas-solid contacting efficiency is achieved for an optimum transfer of mass and heat as would occur in practice by the use of circulating fluidized bed (CFB) reactors [33]. The small particle size allows us also to dismiss the possible effects on the CaO conversion rate caused by intra-particle diffusion resistance that would be important only for particles of size larger than about 300 μm [35].

Particle size distributions (PSD) of the samples before and after being subjected to the carb/calc cycles were obtained using a Mastersizer 2000 (Malvern Instruments Ltd.) instrument, Prior to measuring the PSD, powder samples were dispersed in 2-propanol (as recommended for Ca-based materials according to ISO 14887) and sonicated for 5 seconds just to loosen the particle aggregates formed by van der Waals forces [1].

X-Ray diffractograms of thermally pretreated samples were registered in the 2θ range from 5º to 90º using a Panalytical X'Pert Pro diffractometer working at 45 kV and 40 mA, using CuKα radiation and equipped with an X'Celerator detector and a graphite diffracted beam monochromator.

.

3. Results and discussion

3.1 Effect of thermal pre-treatment on multicycle CO_2 capture of limestone and dolomite

Carbonation/calcination cycles were carried out using the following experimental conditions; (i) an initial thermal pretreatment during which the temperature was linearly increased up to 900 ºC at different rates, (ii) carbonation stages carried out at 650 ºC under a 15% CO_2 / 85% air (vol/vol) atmosphere for 5 minutes and (iii) calcination stages for sorbent regeneration carried out at 900 ºC under a 70% CO_2 / 30% air (vol/vol) atmosphere for 5 minutes (a typical CO_2 concentration in the calciner reactor will be between 70% and 75%) [36]. Transition between carb/calc stages were performed by heating/cooling at 300 ºC/min in order to mimic as closely as possible the rapid transitions that would occur in the practical application when the materials are rapidly circulated between the calciner and carbonator reactors.

The initial thermal treatment was carried out at three different heating rates (1, 10 and 300 ºC/min) under high CO_2 concentration (70% CO_2/30% air vol/vol). In practice, the initial batch of solids to be used in the CaL process would be first calcined for a long period as the temperature is slowly increased. On the other hand, the make-up flow of fresh CaO precursor (either limestone or dolomite) that is directly fed into the calciner during continuous operation would experience first calcination by a quick increase of temperature from ambient to the calciner temperature albeit this sudden rise of temperature could be modulated by using residual heat for preheating the makeup flow in order to mitigate the energy penalty [2]. The practical question to be addressed in this paper is whether a change of the precursor preheating rate would have any effect on its multicycle CO_2 capture behaviour. As will be seen, the behaviour of limestone derived CaO in subsequent carb/calc cycles depends critically on this pre-heating rate if a reduced calcination temperature (T=900ºC, which is 30-50ºC below those typically employed in pilot-scale plants) is used for regeneration. In contrast, the fundamental mechanism of dolomite decomposition under CO_2 allows for its multicycle CO_2 capture behaviour to be pretty insensitive to the precalcination heating rate.

Figures 1 and 2 show the time evolution of temperature and sample weight % during precalcination and the subsequent carb/calc cycles for natural limestone and dolomite,

respectively. The thermograms shown in Figure 1 demonstrate that full decarbonation of fresh limestone cannot be attained by precalcination up to just 900 ºC. Only after a number of carb/calc cycles depending on the first calcination preheating rate, CaO becomes completely available for carbonation. As well known, decarbonation of limestone is heavily hindered by the presence of CO_2 at high concentration in the calcination environment [11, 35, 37-39]. Thus, temperatures well above the equilibrium temperature are required to attain full decarbonation in short residence times (T_{eq}=871ºC in the calcination atmosphere of our experiments). As seen in Fig. 1, complete decarbonation is achieved in our tests only after five, nine and fifteen carb/calc cycles for the samples precalcined at 300, 10 and 1 ºC/min, respectively. The behaviour of limestone along the carb/calc cycles is therefore clearly correlated to the heating rate during first calcination. As the preheating rate is decreased limestone decarbonation is further hindered, which severely hampers the sorbent capture capacity in the first cycles.

In contrast with the strong dependence of limestone CO_2 capture multicycle behaviour on the preheating rate, dolomite exhibits a quite different performance. As illustrated in Figure 2, almost full regeneration of CaO is achieved from the 1st cycle regardless of the preheating rate. Figure 2 shows also a characteristic feature of dolomite decomposition, which takes place during the precalcination stage. While limestone ($CaCO_3$) decomposition occurs by a single step process, with $CaCO_3$ decomposing into CaO and CO_2, dolomite undergoes a two-step process under the presence of CO_2 in the calcination environment [32, 40, 41]. According to a recent in-situ XRD study [21], dolomite decomposition is initiated by a direct conversion into MgO and CaO at temperatures around 700ºC independently of the CO_2 concentration in the calcination environment. The nascent CaO nanocrystals become at this temperature immediately recarbonated, which gives rise to a nanocrystalline $CaCO_3$ that subsequently decarbonates at a higher temperature depending on the CO_2 partial pressure. Thermal decomposition of this fresh $CaCO_3$ under CO_2 obeys to thermodynamic equilibrium as limestone but is characterized by a much faster kinetics [21]. Therefore, as seen in Figure 2, two mass loss events are observed in the precalcination stage of dolomite that correspond to the following reactions [21, 32]:

$$CaMg(CO_3)_2 \rightarrow CaO + MgO + 2CO_2 \rightarrow CaCO_3 + MgO + CO_2 \quad (1)$$

$$CaCO_3 + MgO \rightarrow CaO + CO_2 + MgO \quad (2)$$

As will be discussed ahead in more detail, the mechanism of dolomite decomposition under CO_2 is responsible for the negligible effect of the precalcination heating rate on its multicycle CO_2 capture behaviour.

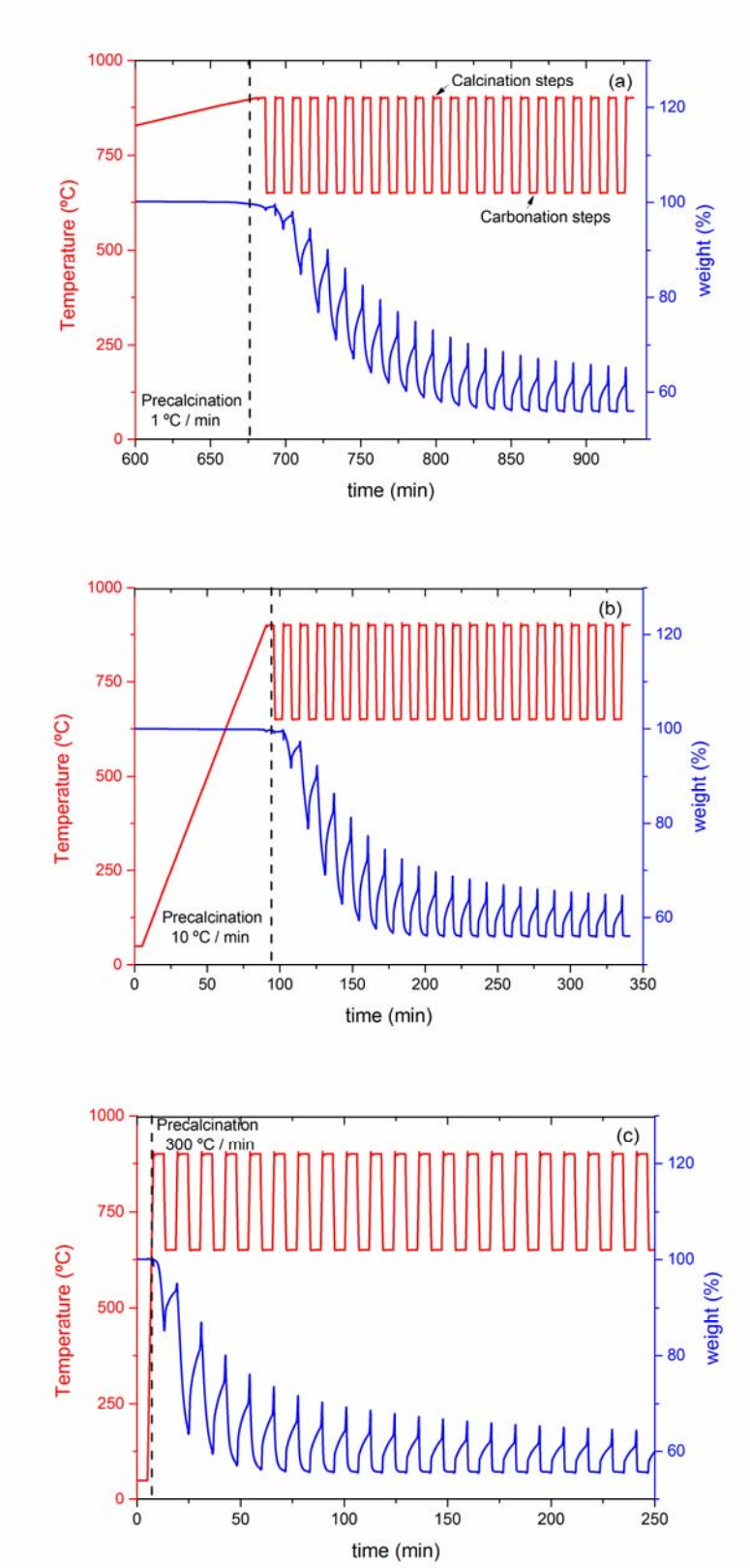

Figure 1. Time evolution of weight % and temperature during multicycle carbonation/calcination of limestone after precalcination at different heating rates: (a) 1ºC/min; (b) 10ºC/min; (c) 300ºC/min. Carbonations at 650 ºC in 15% CO_2 / 85% air (vol/vol) for 5 min and calcinations at 900 ºC in 70% CO_2 / 30% air (vol/vol) for 5 min.

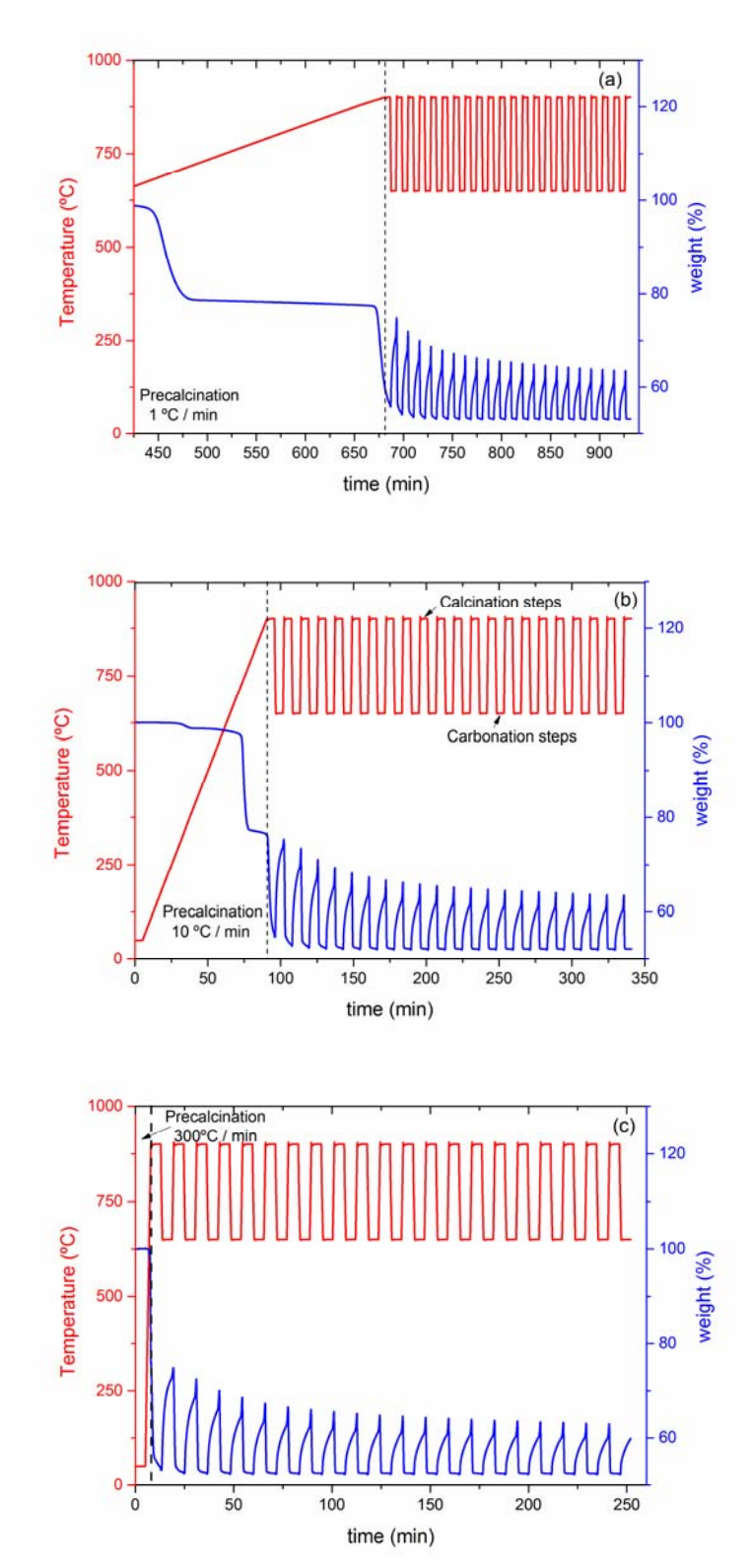

Figure 2. Time evolution of weight % and temperature during multicycle carbonation/calcination of dolomite after precalcination at different heating rates: (a) 1ºC/min; (b) 10ºC/min; (c) 300ºC/min. Carbonations at 650 ºC in 15% CO_2 / 85% air (vol/vol) for 5 min and calcinations at 900 ºC in 70% CO_2 / 30% air (vol/vol) for 5 min.

3.2 Multicycle CO_2 Capture Capacity and CaO Conversion

For practical purposes, the multicycle performance of both sorbents should be compared in terms of their CO_2 capture capacity CC_N, defined as the ratio of CO_2 captured mass to initial sorbent mass in each cycle. Figure 3 shows the capture capacity obtained for both limestone and dolomite as a function of cycle number and for the different heating rates used during precalcination.

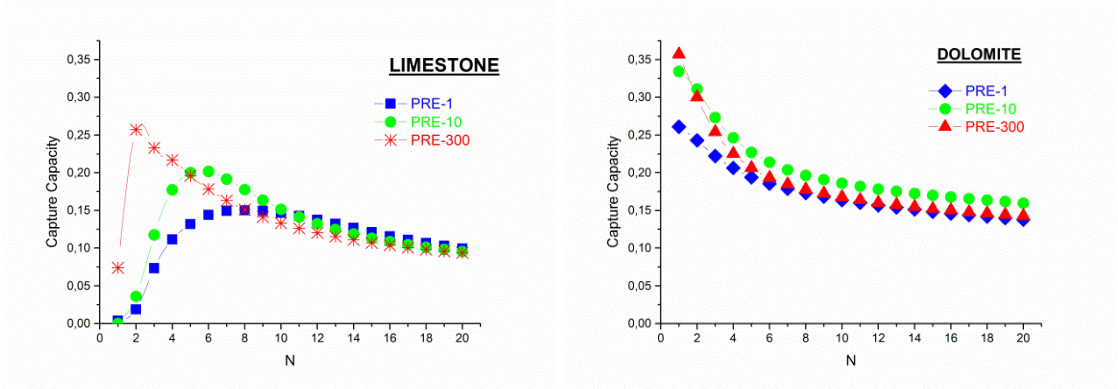

Figure 3. Capture capacity versus cycle number obtained for limestone and dolomite precalcined at different heating rates as indicated; 1ºC/min (PRE-1), 10ºC/min (PRE-10) and 300ºC/min (PRE-300)

As was inferred from Figs 1 and 2, the heating rate during precalcination of limestone has a strong influence on its multicycle capture capacity behaviour, especially during the first carb/calc cycles. Due to incomplete decarbonation in the first cycles, only a small fraction of CaO becomes available for CO_2 capture, hence the capture capability is severely hampered in the first loops. Curtailment of the capture capacity becomes particularly relevant if the sample is very slowly preheated. As the number of cycles is increased, limestone is progressively decarbonated in each calcination stage, which gives rise to an increasing fraction of CaO available and therefore an increase of the capture capacity. Once limestone is fully decarbonated, a maximum of the capture capacity is reached after which it decreases with the number of cycles due to the progressive CaO deactivation caused by sintering. After about 10 cycles, the memory on the incomplete precalcination stage is lost and the capture capacities of the three limestone samples converge to similar values as seen in Fig 3.

In contrast with the behaviour observed for limestone, the much faster decarbonation kinetics of dolomite in the precalcination stage yields a high capture capacity from the first cycle, which is followed by a steady decrease as caused by sorbent deactivation. Interestingly, unlike for limestone, the multicycle capture capacity of the dolomite derived sorbent is almost insensitive

to the precalcination heating rate. Moreover, as can be seen in Figure 3, dolomite shows a superior capture performance as compared to limestone despite the presence of MgO grains that remain inert to carbonation under the CaL process conditions.

A further useful parameter to analyse the multicycle capture behaviour of the sorbents is CaO conversion (Fig. 4), defined as the ratio of CaO mass converted to $CaCO_3$ to the CaO mass before carbonation. CaO conversion is thus a measure of the reactivity of CaO grains towards carbonation. As seen in Fig. 4, the conversion of dolomitic CaO after 20 cycles is more than twice that of limestone derived CaO. The decay of CaO conversion with the number of cycles can be generally well fitted by the following semi-empirical equation [42]:

$$X_N = X_r + \frac{X_1}{k(N-1) + (1 - X_r/X_1)^{-1}}; \qquad (N = 1,2,\dots) \qquad (3)$$

where N is the cycle number, X_1 is CaO conversion in the first cycle, k is the deactivation constant and X_r is the residual conversion, which is asymptomatically approached after a very large number of cycles. Most of TGA data obtained for natural limestones can be reasonably well fitted using Eq. (3), yielding a residual conversion of about 0.07-0.08 and a deactivation constant k close to 0.5 [42, 43]. These values are key to process simulations and economic analyses dealing with the integration of the CaL process into fossil fuel thermal plants [8, 44]. The results obtained from the fit of this equation to experimental data obtained in our work are summarized in Table 1 (best fit curves are shown in Figure 4). Due to the anomalies in limestone curves produced by incomplete decarbonation during the first cycles, Eq (3) can only properly fit to CaO conversion data from the cycle at which full CaO regeneration is achieved. It must be noted that the poor conversion in these first cycles is a serious drawback for the process since it would imply that the capture efficiency of the makeup limestone flow fed into the calciner is severely compromised. Moreover, the residual conversion is decreased as precalcination is further slowed down. On the other hand, dolomite experimental data are all well fitted by Eq. (3) with remarkably good correlation coefficients from the first cycle. Moreover, as seen in table 1, the residual conversion of dolomitic CaO is more or less independent of the precalcination rate and much higher than that of lime for the same conditions, which indicates a superior reactivity of dolomitic CaO as compared to CaO derived from limestone.

TABLE 1. Deactivation constant k, residual conversion X_r and correlation coefficient r^2 resulting for the fitting of experimental data shown in Figure 3 to Eq (3) for limestone and dolomite precalcined at different heating rates; 1ºC/min (PRE-1), 10 ºC/min (PRE-10) and 300 ºC/min (PRE-300):

	X_r	k	r^2
Limestone PRE-1	0.003 ± 0.010	0.055 ± 0.007	0.999
Limestone PRE-10	0.032 ± 0.005	0.124 ± 0.009	0.998
Limestone PRE-300	0.049 ± 0.002	0.245 ± 0.005	0.999
Dolomite PRE-1	0.232 ± 0.002	0.355 ± 0.010	0.999
Dolomite PRE-10	0.264 ± 0.007	0.420 ± 0.030	0.994
Dolomite PRE-300	0.247 ± 0.004	0.581 ± 0.021	0.998

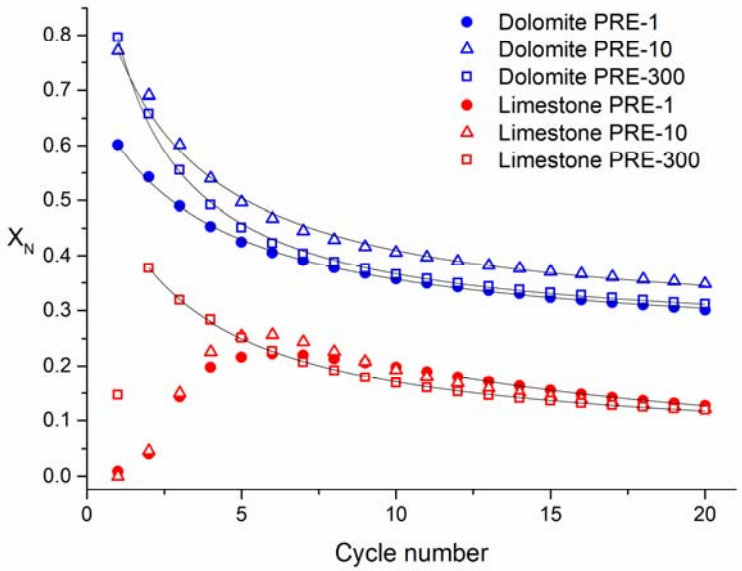

Figure 4. CaO conversion X_N versus cycle number obtained for limestone and dolomite precalcined at different heating rates; 1ºC/min (PRE-1), 10 ºC/min (PRE-10) and 300 ºC/min (PRE-300). The solid lines are best fit curves of Eq. (3) to the data.

3.3 Influence of crystal growth and sintering on CaO conversion

The contrasting multicycle capture behaviour of limestone and dolomite can be rationalized in terms of the crystallinity of the CaO structure that stems from decomposition. As previously reported, decarbonation kinetics of highly crystalline $CaCO_3$ is much slower than that of nanocrystalline $CaCO_3$ [45, 46]. Precalcination at a slow heating rate in a high CO_2 concentration environment (annealing) would expectedly promote the growth of large, defect-free $CaCO_3$ crystals [21, 45-47]. Accordingly, the experimental results shown in Figure 1

demonstrate that there is a clear correlation between limestone decarbonation kinetics and the heating rates used in the precalcination. Thus, the lower the heating rates, the slower decarbonation kinetics.

In order to further explore the relationship between crystallinity and precalcination heating rates, a sample of limestone was heated up under a pure CO_2 atmosphere to 890ºC, just below the equilibrium temperature (~895ºC) at a very slow heating rate of 1ºC/min. XRD diffraction patterns obtained for this slowly preheated limestone and fresh limestone are shown in Figure 5a. As can be seen, the main diffraction peak of the calcite crystal structure, corresponding to the (211) Bragg reflection peak, appears noticeably sharper for the sample preheated at 1 ºC/min indicating a much larger coherent crystal length, which would hinder the decarbonation kinetics as shown in Figure 1. As seen above, the decarbonation kinetics of dolomite and subsequent multicycle capture behaviour appear to be quite insensitive to the different precalcination heating rates in clear contrast with the case of limestone. This could be attributed to the fact that $CaCO_3$ in dolomite is formed just after the first stage decomposition of dolomite by immediate recarbonation of the nascent CaO nanocrystals, which gives rise to a nanocrystalline calcite structure consisting of small crystals of about 50 nm as measured in [21] by in situ XRD analysis. Figure 5b shows the XRD diffractograms obtained for the limestone and dolomite samples calcined at 1ºC/min up to 890 ºC under pure CO_2. As would be expected, the fresh $CaCO_3$ derived from dolomite half decomposition is noticeably less crystalline, which explains its enhanced decarbonation kinetics as compared to limestone. Consequently, the CaO derived from decomposition of this highly reactive $CaCO_3$ derived from dolomite also displays a high reactivity towards carbonation from the very first cycle as illustrated in Figures 3 and 4. Nonetheless, the dolomite heated up to 890ºC at a slow heating rate of 1ºC/min still undergoes significant crystal growth since the coherent domain size is over 100 nm and cannot be accurately determined by Scherrer method. That crystal growth results in slower decarbonation kinetics as can be observed in Figure 2a and 3 where the decarbonation in the first cycle is not yet fully achieved unless the dolomite is heated up at 300ºC/min. In any case, dolomite decarbonation under identical thermal treatment remains always much faster than limestone. This enhanced decarbonation kinetics constitutes an important advantage since, given the limited lifetime of the makeup flow of fresh material fed into the calciner, it is of paramount importance to maximize the CaO carbonation reactivity from the first cycle at a reduced calcination temperature. As seen in our work this is possible for dolomite by operating the calciner at 900ºC whereas in the case of limestone the calciner temperature has to be increased up to 930-950ºC, which enhances further CaO deactivation [48].

The improved performance of dolomite when the number of cycles is large can be attributed to the stabilizing effect of the inert MgO skeleton as previously reported [21] which hinders the

aggregation and subsequent sintering of the nascent CaO crystals during the $CaCO_3$/CaO transformation. The superior resistance of dolomite to sintering can be also rationalized from the particle size distributions (PSD), as measured by laser diffractometry, for untreated and cycled samples (Figure 6). Light scattering is used in this technique to measure the size distribution profile of powder particles pre-dispersed in a liquid by sonication. As can be seen, the PSD distribution shifts notably to larger particle sizes in the case of limestone, which indicates promoted sintering. On the other hand, the PSD measured for dolomite remains almost unchanged after repeated carb/calc cycles. Additionally, Figure 7 shows SEM micrographs for dolomite and limestone samples obtained after the 20 carb/calc cycles. It is clearly observed in the SEM micrograph that the CaO grains in limestone are markedly sintered as compared with those in dolomite, which still retains a relatively porous structure after the cycles. Figure 7d shows an area of the sorbent where EDX analysis was performed to identify MgO and CaO grains. As the EDX spectra in 7e and 7f shows, area 2, which is richer in small particles yields a Ca/Mg atomic ratio slightly smaller than one whereas area 1, corresponding to a sintered particle appears enriched in Ca atoms. This confirms that the larger, sintered particles correspond to CaO which are prone to sintering in the CO_2 rich environment. This also helps explaining the much higher CaO conversion values exhibited by dolomite since the porous structure allows a higher CaO surface area to be readily available for reaction controlled carbonation in short residence times. On the other hand, the notable increase of CaO grain size due to enhanced sintering in the case of limestone limits drastically the CaO surface area available for fast reaction controlled carbonation. Nevertheless, MgO particles slowly segregate from the CaO grains by solid-state diffusion so that the stabilizing role of the MgO skeleton is eventually lost. This segregation is clearly observed in the SEM pictures and also revealed by EDX mappings as seen in Figure 8.

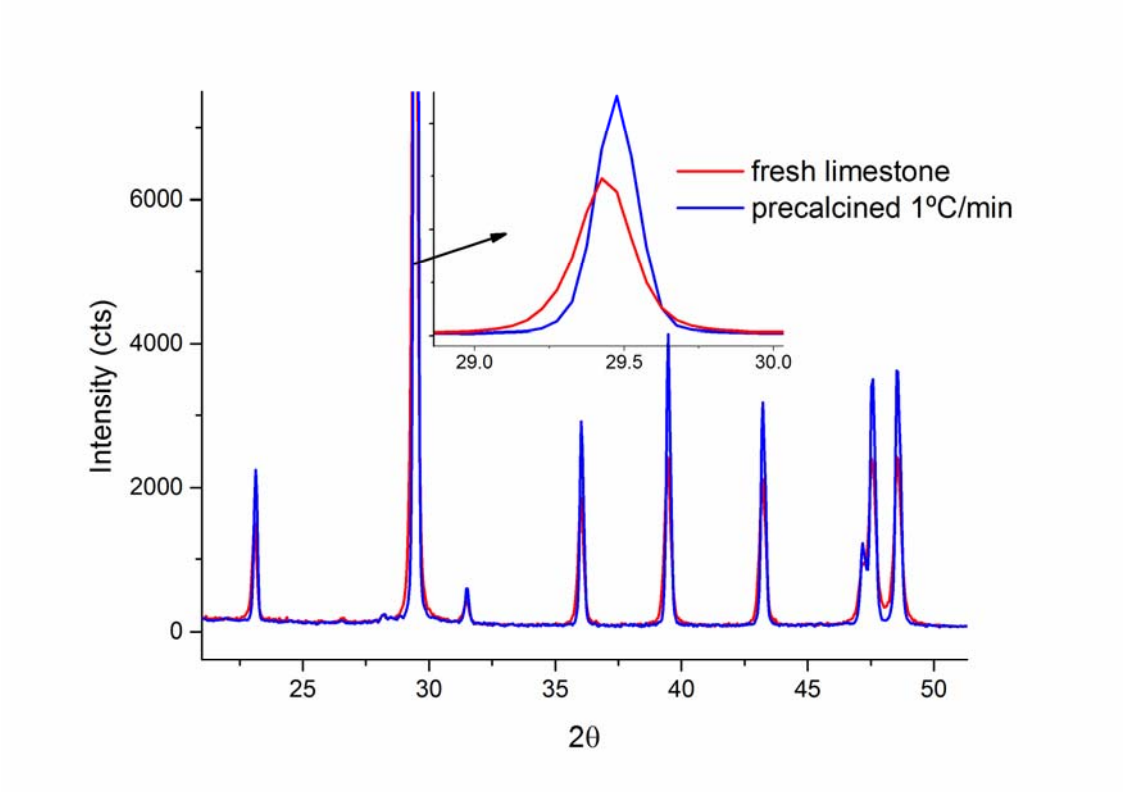

Figure 5a. XRD diffractograms of raw limestone and limestone heated at 1ºC/min up to 890ºC under pure CO_2.

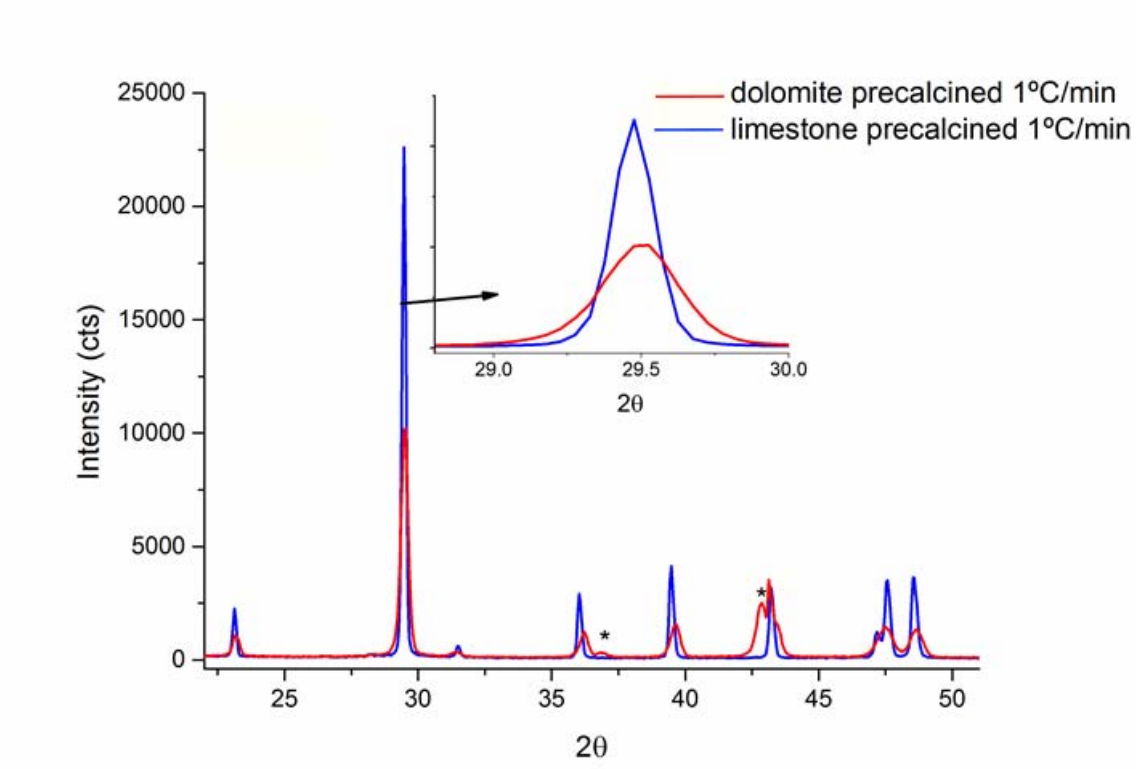

Figure 5b. XRD diffractograms of dolomite and limestone samples heated at 1ºC/min up to 890ºC under CO_2.

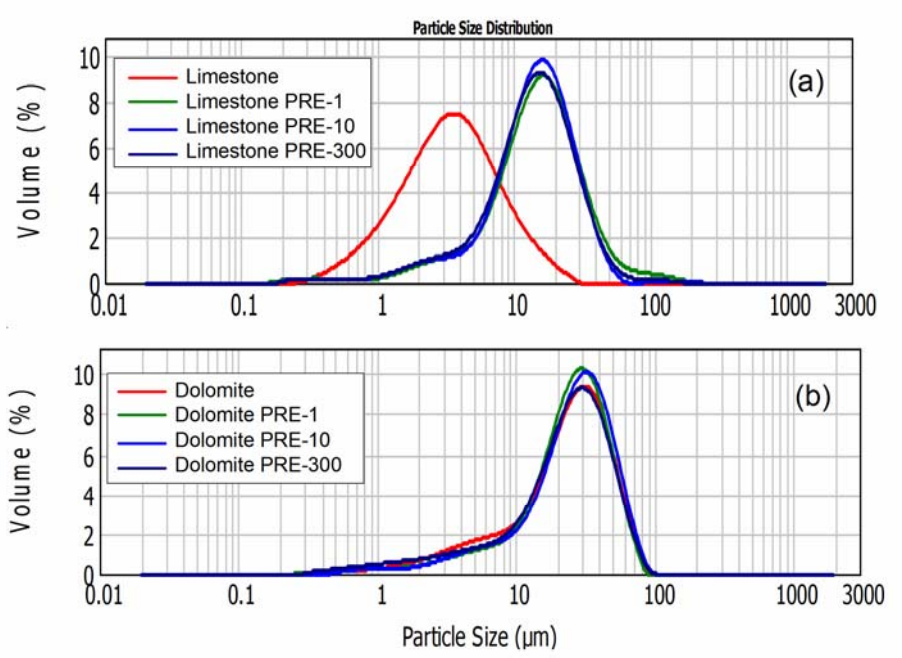

Figure 6. Particle size distributions (PSD) obtained for the raw sorbent precursors (limestone and dolomite) and after 20 carb/calc cycles. Curves in (a) correspond to limestone whereas (b) correspond to dolomite.

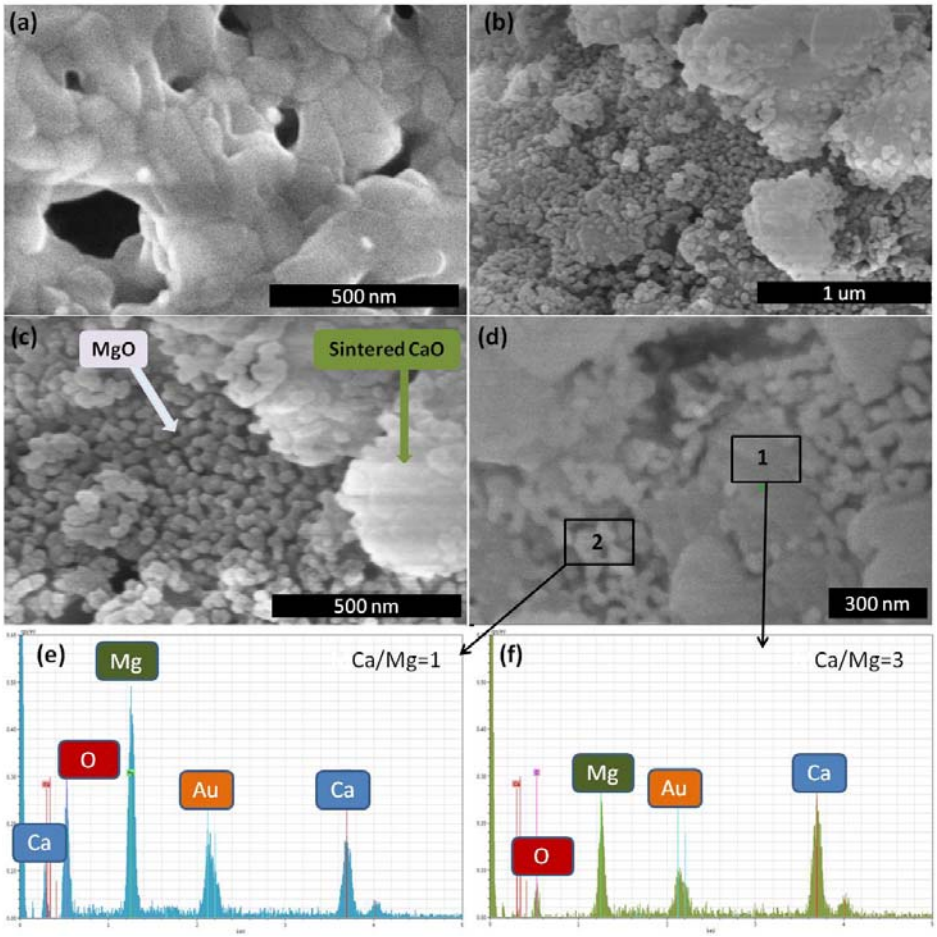

Figure 7. SEM micrographs of (a) limestone and (b,c) dolomite after 20 carb/calc cycles. Precalcination was carried out at 300 ºC/min in 70% CO_2/30% air atmosphere. (d) is a SEM micrograph showing the areas where the EDX analysis in (e) and (f) were performed.

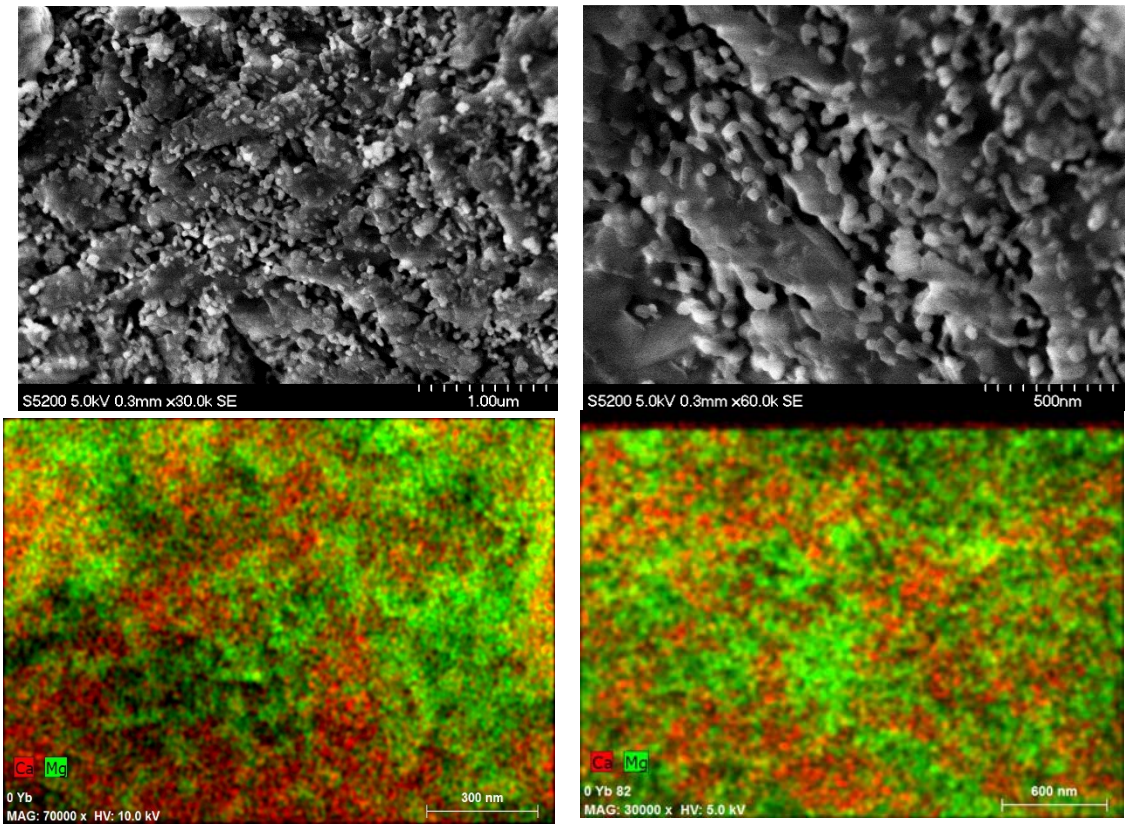

Figure 8. SEM micrographs of calcined dolomite (10ºC/min under CO_2) and EDX mappings obtained from these pictures.

3.4 Role of solid-state diffusion controlled carbonation on overall capture

It is generally accepted that carbonation of CaO grains occurs through two differentiated phases consisting of a fast reaction-controlled (FR) stage followed by a much slower solid state diffusion (SD) stage. The FR stage is due to the gas-solid reaction of CO_2 with CaO on the surface of the grains [49, 50] that leads to the formation of a thin layer of $CaCO_3$, which normally takes place in short periods of time at the carbonation temperature of the CaL process for CO_2 capture. On the other hand, the following SD stage requires the counter-diffusion of CO_3^{2-} and O^{2-} ions through the previously formed carbonate layer, which leads to a notable reduction of the reaction rate [51-53]. Carbonation in the SD phase is usually considered as negligible in the typically short residence times of the solids in the carbonator (of a few minutes). Thus, carbonator models for the integration of the CaL process into fossil fuel power plants generally dismiss SD carbonation [8, 54]. It must be stressed however that this assumption is based upon TGA results in which calcination is carried out under low CO_2 partial pressure. At realistic CaL conditions for CO_2 capture involving calcination under high CO_2 partial pressure, the SD phase yields a relevant contribution to carbonation in short residence times (as will be seen also from our results below) [55]. Thus, the solids residence time in the

carbonator has an important effect on the capture efficiency predicted by carbonator models if carbonation in the SD phase is taken into account [56].

Figure 9 shows in detail the temperature and weight % time evolution during the 8^{th}, 12^{th} and 20^{th} carb/calc cycle for both limestone and dolomite (precalcined at 10 ºC/min). As can be seen, the FR and SD carbonation phases can be clearly distinguishable. It may be also observed that carbonation in the SD phase significantly contributes to the overall carbonation in the 5min period of our experiments. Interestingly, carbonation during the FR stage is fairly similar for limestone and dolomite so at first glance it would appear that porosity and surface area alone does not explain by itself the enhanced CaO conversion of dolomite. Nevertheless, it should be stressed the difference between CO_2 capture capacity and CaO conversion. Since dolomite is composed of reacting CaO and inert MgO particles, the amount of active material is actually much smaller in dolomite. Thus, a similar mass gain during the FR stage implies a much higher proportion of existing CaO converting into $CaCO_3$, what could be explained in terms of the higher porosity of the calcined dolomite that allows for a higher proportion of CaO readily available for CO_2 capture. Moreover, during the SD stage dolomite derived CaO exhibits a remarkably faster kinetics, resulting in an overall higher capture capacity. This difference in the capture capacity in favour of dolomite is progressively enlarged with the number of cycles, which explains why deactivation of dolomitic CaO is significantly attenuated as compared to lime. Thus, the improved CO_2 capture capacity of dolomite is due to the greatly promoted carbonation in the solid state diffusion phase. As would be expected, solid state diffusion is promoted by impurities and lattice defects [11, 47, 57-66], hence the nanocrystalline CaO grains and the presence of MgO inert grains in decomposed dolomite favour carbonation in the solid state diffusion controlled phase. Additionally, the decarbonation rate of dolomite is significantly faster during the first cycles since crystal defects also promote the diffusion of desorbed CO_2 and facilitates the structural transformation step at CO_2 partial pressures close to equilibrium [11]. Nevertheless, the difference in decarbonation rates between the limestone and dolomite derived sorbents decreases as the sample undergoes repeated carb/calc arguably because of the progressive segregation of the MgO/CaO grains as inferred from the SEM-EDX analysis.

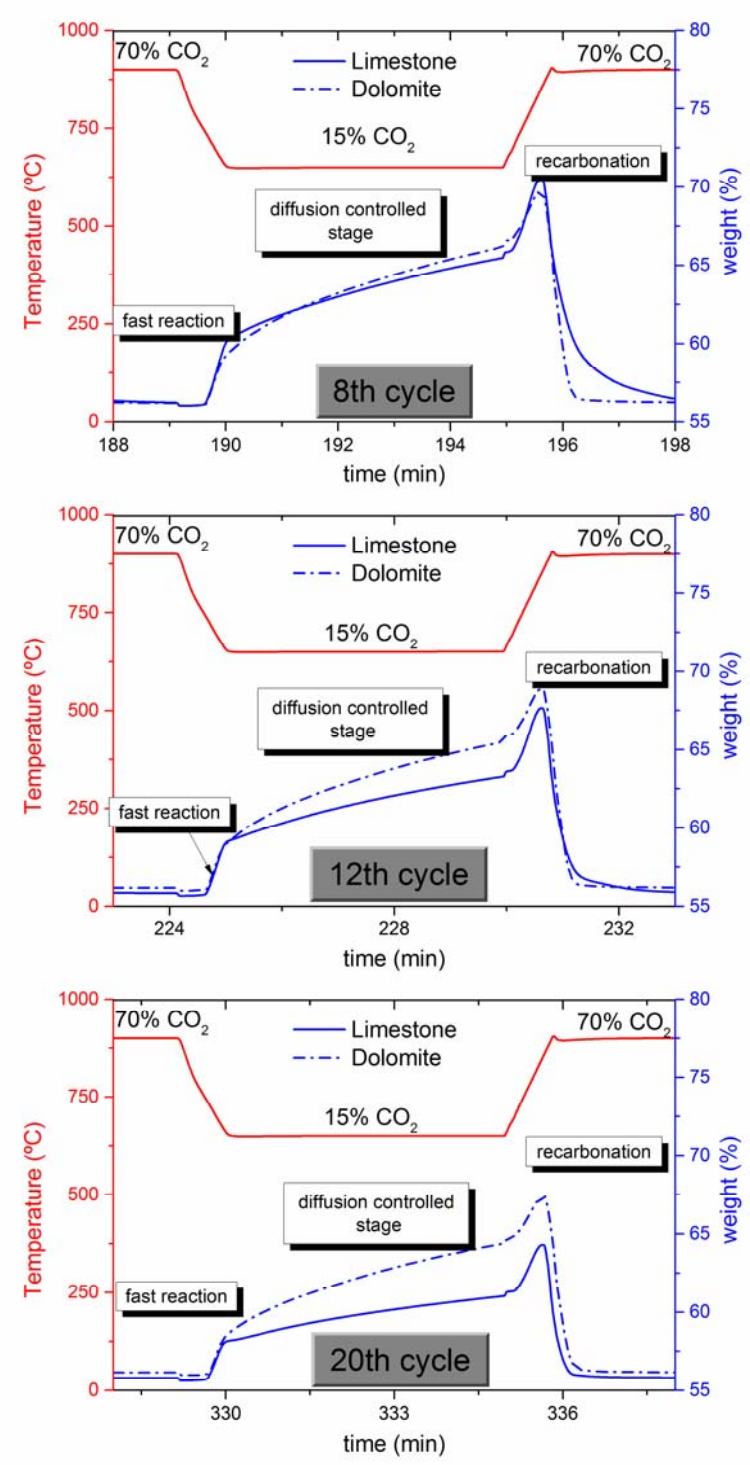

Figure 9. Thermograms obtained for the 8th, 12th and 20th carb/calc cycle of dolomite and limestone samples (precalcined at 10ºC/min). The fast reaction controlled and the slow diffusion controlled stages are indicated, as well as the transitory recarbonation that occurs during the quick transition to the calcination step, carried out under 70% CO_2/30% air vol/vol atmosphere.

Figure 10 shows the evolution with the number of cycles of the ratio of CaO conversion in the SD phase to conversion in the FR phase (X_{SD} / X_{FR}). As can be observed, both limestone and dolomite present X_{SD} / X_{FR} ratios over 1. Thus, it may be concluded that solid state diffusion

carbonation is more relevant to the overall conversion than the fast stage for residence times of the solids in the carbonator of just a few minutes. This effect becomes even more pronounced in the case of dolomite, for which the X_{SD}/X_{FR} ratio is even increased with the cycle number.

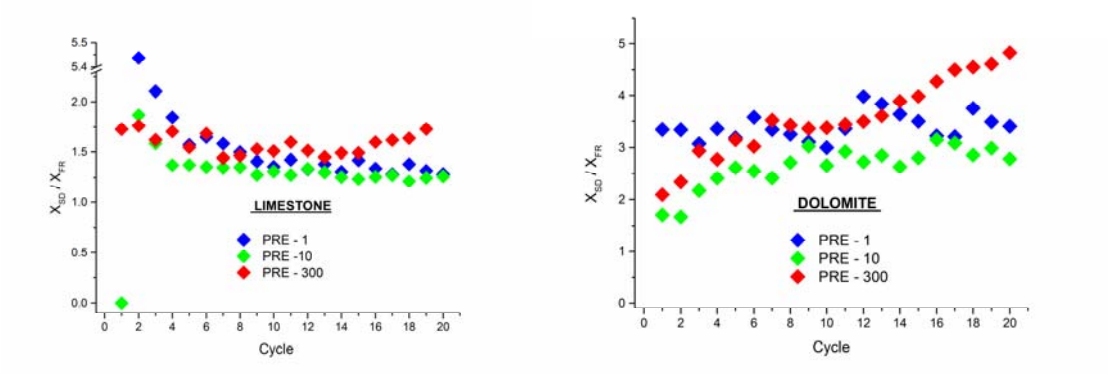

Figure 10. Ratio between CaO conversion in the solid state diffusion stage to conversion in the fast reaction stage (X_{SD} / X_{FR}) versus the cycle number obtained for (a) dolomite and (b) limestone for samples precalcined at 1, 10 and 300ºC/min (PRE-1, PRE-10 and PRE-300 respectively).

4. Conclusions

In this work, the effect of different first calcination heating rates on the multicycle CO_2 capture behaviour of limestone and dolomite derived CaO is studied. The tests have been carried out under realistic Calcium-Looing (CaL) operation conditions as regards calcination under high CO_2 concentration at high temperature and quick transitions between carbonation and calcination stages. The sorbents have been regenerated by calcination at 900 ºC, which is below the temperature typically used (~930-950ºC) for limestone calcination in CaL pilot-scale plants to attain full decarbonation in short residence times as required in practice. Under this reduced calcination temperature, which would bring about an important reduction in the energy penalty of the technology, it is shown that dolomite exhibits an enhanced multicycle capture capacity performance, which can be attributed to the stability provided by the inert MgO skeleton formed after dolomite decomposition in the precalcination stage. MgO grains hinder aggregation and

sintering of CaO grains and help preserving a nanocrystalline CaO structure wherein carbonation during the solid state diffusion controlled carbonation phase is promoted. An interesting feature of dolomite is a remarkable lack of sensitivity to different precalcination treatments as compared to limestone, whose capture capacity along subsequent cycles strongly depends on the heating rate at which precalcination is carried out. Thus, slow calcination of limestone in a CO_2 rich atmosphere promotes sintering and crystal growth thereby forming a less reactive $CaCO_3$ structure that requires longer times to decarbonate into CaO and consequently exhibits a severely reduced capture capacity during the first carbonation cycles. This behaviour is not observed for dolomite, which can be explained from its fundamental mechanism of decomposition under CO_2. Thus, aggregation and sintering of the nascent $CaCO_3$ nanocrystals produced after dolomite half-decomposition is mitigated by the inert MgO grains allowing for faster decarbonation kinetics, which leads to almost complete decarbonation from the very first cycle regardless of the heat pretreatment.

Altogether, the advantage of using dolomite over limestone in the CaL process for CO_2 capture is threefold from the perspective of its multicycle capture performance; a lower effective calcination temperature that serves to mitigate the energy penalty of the technology, an attenuated deactivation that would allow for longer lifetime of the sorbents in the cycle thus reducing the need of makeup flow, and enhanced carbonation and decarbonation kinetics that maximize the CO_2 capture capacity from the very first cycle. Finally, the enhanced kinetics during the solid-state controlled carbonation phase, especially observed in the case of dolomite, emphasizes the need of further exploring the feasibility of increasing the residence time in the carbonator as a possible strategy to mitigate the penalty caused by the CaL integration into fossil fires power plants.

Acknowledgements

This work was supported by the Andalusian Regional Government Junta de Andalucía (Contracts FQM-5735, TEP-7858 and TEP-1900), Spanish Government Agency Ministerio de Economia y Competitividad and FEDER funds (Contracts CTQ2014-52763-C2-1-R and CTQ2014-52763-C2-2-R). One of the authors (PESJ) is supported by a Marie Curie–Junta de Andalucía Postdoc Talentia grant. The authors also thank VPPI-US for AP current contract. We gratefully acknowledge the XRD, SEM and Functional Characterization Services of the Innovation, Technology and Research Centre of the University of Seville (CITIUS).

5. References

1. Blamey, J., et al., *The calcium looping cycle for large-scale CO_2 capture.* Progress in Energy and Combustion Science, 2010. **36**(2): p. 260-279.
2. Perejón, A., et al., *The Calcium-Looping technology for CO2 capture: On the important roles of energy integration and sorbent behavior.* Applied Energy, 2016. **162**: p. 787-807.
3. Wang, Q., et al., *CO2 capture by solid adsorbents and their applications: Current status and new trends.* Energy and Environmental Science, 2011. **4**(1): p. 42-55.
4. Liu, W., et al., *Performance enhancement of calcium oxide sorbents for cyclic CO 2 capture-a review.* Energy and Fuels, 2012. **26**(5): p. 2751-2767.
5. Fan, L.S., et al., *Chemical looping processes for CO<inf>2</inf> capture and carbonaceous fuel conversion - Prospect and opportunity.* Energy and Environmental Science, 2012. **5**(6): p. 7254-7280.
6. Wang, J., et al., *Recent advances in solid sorbents for CO2 capture and new development trends.* Energy and Environmental Science, 2014. **7**(11): p. 3478-3518.
7. Romano, M.C., et al., *Process simulation of Ca-looping processes: review and guidelines.* Energy Procedia, 2013. **37**: p. 142-150.
8. Romano, M.C., *Modeling the carbonator of a Ca-looping process for CO_2 capture from power plant flue gas.* Chemical Engineering Science, 2012. **69**(1): p. 257-269.
9. Arias, B., et al., *Demonstration of steady state CO2 capture in a 1.7 MWth calcium looping pilot.* International Journal of Greenhouse Gas Control, 2013. **18**: p. 237-245.
10. Strohle, J., et al., *Carbonate looping experiments in a 1 MWth pilot plant and model validation.* Fuel, 2014. **127**: p. 13-22.
11. Valverde, J.M., P.E. Sanchez-Jimenez, and L.A. Perez-Maqueda, *Limestone calcination nearby equilibrium: kinetics, CaO crystal structure, sintering and reactivity.* Journal of Physical Chemistry C, 2015. **119**(4): p. 1623-1641.
12. Ylätalo, J., et al., *Modeling of the oxy-combustion calciner in the post-combustion calcium looping process.* Fuel, 2013. **113**: p. 770-779.
13. Ylätalo, J., et al., *Model based scale-up study of the calcium looping process.* Fuel, 2014. **115**: p. 329-337.
14. Rodriguez, N., et al., *Heat requirements in a calciner of $CaCO_3$ integrated in a CO_2 capture system using CaO.* Chemical Engineering Journal, 2008. **138**(1–3): p. 148-154.
15. Charitos, A., et al., *Experimental validation of the calcium looping CO_2 capture process with two circulating fluidized bed carbonator reactors.* Industrial & Engineering Chemistry Research, 2011. **50**(16): p. 9685-9695.
16. Lisbona, P., A. Martínez, and L.M. Romeo, *Hydrodynamical model and experimental results of a calcium looping cycle for CO2 capture.* Applied Energy, 2013. **101**: p. 317-322.
17. Coppola, A., et al., *Fluidized bed calcium looping cycles for CO2 capture under oxy-firing calcination conditions: Part 1. Assessment of six limestones.* Chemical Engineering Journal, 2013. **231**: p. 537-543.
18. Martínez, A., et al., *Operation of a cyclonic preheater in the Ca-Looping for CO_2 capture.* Environmental Science & Technology, 2013. **47**(19): p. 11335-11341.
19. Diego, M.E., et al., *The impact of calcium sulfate and inert solids accumulation in post-combustion calcium looping systems.* Fuel, 2013. **109**: p. 184-190.

20. García-Labiano, F., et al., *Calcium-based sorbents behaviour during sulphation at oxy-fuel fluidised bed combustion conditions.* Fuel, 2011. **90**(10): p. 3100-3108.
21. Valverde, J.M., et al., *Thermal decomposition of dolomite under CO2: Insights from TGA and in situ XRD analysis.* Physical Chemistry Chemical Physics, 2015. **17**(44): p. 30162-30176.
22. Valverde, J.M., P.E. Sanchez-Jimenez, and L.A. Perez-Maqueda, *Effect of heat pretreatment/recarbonation in the Ca-Looping process at realistic calcination conditions.* Energy & Fuels, 2014. **28**(6): p. 4062-4067.
23. Valverde, J.M., et al., *Role of looping-calcination conditions on self-reactivation of thermally pretreated CO_2 sorbents based on CaO.* Energy & Fuels, 2013. **27**(6): p. 3373-3384.
24. Arias, B., et al., *Post-combustion calcium looping process with a highly stable sorbent activity by recarbonation.* Energy & Environmental Science, 2012. **5**(6): p. 7353-7359.
25. Grasa, G., et al., *Determination of CaO carbonation kinetics under recarbonation conditions.* Energy & Fuels, 2014. **28**(6): p. 4033-4042.
26. Valverde, J.M., P.E. Sanchez-Jimenez, and L.A. Perez-Maqueda, *High and stable Co2 capture capacity of natural limestone at Ca-looping conditions by heat pretreatment and recarbonation synergy.* Fuel, 2014. **123**: p. 79-85.
27. Manovic, V. and E.J. Anthony, *Thermal activation of CaO-based sorbent and self-reactivation during CO_2 capture looping cycles.* Environmental Science & Technology, 2008. **42**(11): p. 4170-4174.
28. Valverde, J.M., P.E. Sanchez-Jimenez, and L.A. Perez-Maqueda, *Role of precalcination and regeneration conditions on postcombustion CO_2 capture in the Ca-looping technology.* Applied Energy, 2014. **136**: p. 347-356.
29. Coppola, A., et al., *Fluidized bed calcium looping cycles for CO_2 capture under oxy-firing calcination conditions: Part 2. Assessment of dolomite vs. limestone.* Chemical Engineering Journal, 2013. **231**(0): p. 544-549.
30. Valverde, J.M., P.E. Sanchez-Jimenez, and L.A. Perez-Maqueda, *Ca-looping for postcombustion CO2 capture: A comparative analysis on the performances of dolomite and limestone.* Applied Energy, 2015. **138**: p. 202-215.
31. Wang, K., et al., *Natural dolomite modified with carbon coating for cyclic high-temperature CO2 capture.* Applied Energy, 2016. **165**: p. 14-21.
32. Rodriguez-Navarro, C., K. Kudlacz, and E. Ruiz-Agudo, *The mechanism of thermal decomposition of dolomite: New insights from 2D-XRD and TEM analyses.* American Mineralogist, 2012. **97**(1): p. 38-51.
33. Hanak, D.P., E.J. Anthony, and V. Manovic, *A review of developments in pilot-plant testing and modelling of calcium looping process for CO_2 capture from power generation systems.* Energy & Environmental Science, 2015. **8**(8): p. 2199-2249.
34. Dollimore, D., et al., *The decrepitation of dolomite and limestone.* Thermochimica Acta, 1994. **237**(1): p. 125-131.
35. García-Labiano, F., et al., *Calcination of calcium-based sorbents at pressure in a broad range of CO_2 concentrations.* Chemical Engineering Science, 2002. **57**(13): p. 2381-2393.
36. Martínez, I., et al., *Modelling the continuous calcination of $CaCO_3$ in a Ca-looping system.* Chemical Engineering Journal, 2013. **215–216**(0): p. 174-181.
37. Hyatt, E.P., I.B. Cutler, and M.E. Wadsworth, *Calcium Carbonate Decomposition in Carbon Dioxide Atmosphere.* Journal of the American Ceramic Society, 1958. **41**(2): p. 70-74.
38. Beruto, D., L. Barco, and A.W. Searcy, *CO_2-catalyzed surface-area and porosity changes in high-surface-area cao aggregates.* Journal of the American Ceramic Society, 1984. **67**(7): p. 512-515.

39. Khinast, J., et al., *Decomposition of limestone: The influence of CO_2 and particle size on the reaction rate.* Chemical Engineering Science, 1996. **51**(4): p. 623-634.
40. Haul, R.A.W. and H. Heystek, *Differential thermal analysis of the dolomite decomposition.* American Mineralogist, 1952. **37**(3-4): p. 166-179.
41. Caceres, P.G. and E.K. Attiogbe, *Thermal decomposition of dolomite and the extraction of its constituents.* Minerals Engineering, 1997. **10**(10): p. 1165-1176.
42. Grasa, G.S. and J.C. Abanades, *CO_2 capture capacity of CaO in long series of carbonation/calcination cycles.* Industrial & Engineering Chemistry Research, 2006. **45**(26): p. 8846-8851.
43. Wang, J., et al., *A study on the activity of CaO-based sorbents for capturing CO2 in clean energy processes.* Applied Energy, 2010. **87**(4): p. 1453-1458.
44. Romeo, L.M., et al., *Economical assessment of competitive enhanced limestones for CO_2 capture cycles in power plants.* Fuel Processing Technology, 2009. **90**(6): p. 803-811.
45. Valverde, J.M., P.E. Sanchez-Jimenez, and L.A. Perez-Maqueda, *Calcium-looping for post-combustion CO_2 capture. On the adverse effect of sorbent regeneration under CO_2.* Applied Energy, 2014. **126**: p. 161-171.
46. Valverde, J.M., P.E. Sanchez-Jimenez, and L.A. Perez-Maqueda, *Relevant influence of limestone crystallinity on CO_2 capture in the Ca-Looping technology at realistic calcination conditions.* Environmental Science & Technology, 2014. **48**(16): p. 9882-9889.
47. Borgwardt, R.H., *Sintering of nascent calcium-oxide.* Chemical Engineering Science, 1989. **44**(1): p. 53-60.
48. Ortiz, C., et al., *A new model of the carbonator reactor in the calcium looping technology for post-combustion CO2 capture.* Fuel, 2015. **160**: p. 328-338.
49. Ochs, D., et al., *CO2 chemisorption at Ca and CaO surfaces: a study with MIES, UPS(HeI) and XPS.* Surface Science, 1998. **417**(2–3): p. 406-414.
50. Voigts, F., et al., *The adsorption of CO2 and CO on Ca and CaO films studied with MIES, UPS and XPS.* Surface Science, 2009. **603**(1): p. 40-49.
51. Bhatia, S.K. and D.D. Perlmutter, *Effect of the product layer on the kinetics of the CO_2-lime reaction.* AIChE Journal, 1983. **29**(1): p. 79-86.
52. Sun, Z., et al., *Ionic diffusion through Calcite (CaCO3) layer during the reaction of CaO and CO2.* Chemical Engineering Science, 2012. **81**: p. 164-168.
53. Grasa, G., et al., *Application of the random pore model to the carbonation cyclic reaction.* AIChE Journal, 2009. **55**(5): p. 1246-1255.
54. Alonso, M., et al., *Modelling of a fluidized bed carbonator reactor to capture CO2 from a combustion flue gas.* Chemical Engineering Science, 2009. **64**(5): p. 883-891.
55. Sanchez-Jimenez, P.E., J.M. Valverde, and L.A. Perez-Maqueda, *Multicyclic conversion of limestone at Ca-looping conditions: The role of solid-sate diffusion controlled carbonation.* Fuel, 2014. **127**: p. 131-140.
56. Ortiz, C., et al., *A new integration model of the Calcium Looping technology into coal fired power plants for CO2 capture.* Applied Energy, 2016.
57. Stanmore, B.R. and P. Gilot, *Review—calcination and carbonation of limestone during thermal cycling for CO_2 sequestration.* Fuel Processing Technology, 2005. **86**(16): p. 1707-1743.
58. Milne, C.R., et al., *Calcination and sintering models for application to high-temperature, short-time sulfation of calcium-based sorbents.* Industrial & Engineering Chemistry Research, 1990. **29**(2): p. 139-149.
59. Gleiter, H., *Nanocrystalline materials.* Progress in Materials Science, 1989. **33**(4): p. 223-315.
60. Gleiter, H., *Diffusion in Nanostructured Metals.* physica status solidi (b), 1992. **172**(1): p. 41-51.

61. Tjong, S.C. and H. Chen, *Nanocrystalline materials and coatings.* Materials Science and Engineering: R: Reports, 2004. **45**(1–2): p. 1-88.
62. Heitjans, P. and S. Indris, *Fast diffusion in nanocrystalline ceramics prepared by ball milling.* Journal of Materials Science, 2004. **39**(16-17): p. 5091-5096.
63. Kaur, I., Y. Mishin, and W. Gust, *Fundamentals of Grain and Interphase Boundary Diffusion*. 3rd ed. 1995: Wiley.
64. Martin, M., *Diffusion in Oxides*, in *Diffusion in Condensed Matter*, P. Heitjans and J. Karger, Editors. 2005, Springer. p. 209-247.
65. Anderson, T.F., *Self-diffusion of carbon and oxygen in calcite by isotope exchange with carbon dioxide.* Journal of Geophysical Research, 1969. **74**(15): p. 3918-3932.
66. Anderson, T.F., *Self-diffusion of carbon and oxygen in dolomite.* Journal of Geophysical Research, 1972. **77**(5): p. 857-861.